

A Direct Solution to the Space-Dependent Boltzmann Transport Equation in Silicon

Hongchin Lin, Neil Goldsman and I.D. Mayergoyz

Department of Electrical Engineering
University of Maryland
College Park, MD 20742
(301)405-3648

Abstract: The space-dependent nonequilibrium distribution function is obtained by solving the Boltzmann transport equation for silicon. The Boltzmann equation is expressed as a partial difference/differential equation which incorporates the effects of a non-parabolic band structure, inelastic phonon scattering, as well as spatial variation. The analytical form is then discretized and efficiently solved utilizing both sparse-matrix techniques and SOR type iterations. Agreement with Monte Carlo simulation is obtained.

1. Introduction

In this paper we present a new deterministic method for ascertaining the space-dependent momentum distribution function (SDMDF). The method requires relatively little CPU time to execute, and its results are in agreement with Monte Carlo simulations. To obtain the SDMDF, we build upon an existing technique for solving the Boltzmann transport equation (BTE) which combines analytical approaches involving Legendre polynomials with numerical methods. This new method has already been used for obtaining values for the space-independent distribution function which agree with Monte Carlo simulations[1] and experiment[2]. This approach has also been applied to the quantum-mechanical regime to obtain degenerate distribution functions[3]. Here, the work is extended into the real-space domain by including the spatial derivative of the Boltzmann transport equation in the analysis. The transport model employed is identical to one commonly used in Monte Carlo calculations which includes the effects of non-parabolic band structure, as well as acoustic and intervalley phonon scattering[4]. To solve the space-dependent Boltzmann equation, we first use analytical methods to obtain a linear, second order partial differential/difference equation. This form of the Boltzmann equation is then discretized and solved numerically by employing a sparse-matrix method in the energy domain, and an iterative method in the real-space domain. Once the SDMDF is ascertained, we use it to compute average electron energy, drift velocity, and carrier concentrations as functions of position. Calculated values are in excellent agreement with results from Monte Carlo simulations.

2. Formulation of Space-Dependent Boltzmann Transport Equation

To obtain the space-dependent momentum distribution function (SDMDF) for silicon, we begin with the standard Boltzmann transport equation for electrons in steady state:

$$\frac{1}{\hbar} \nabla_{\mathbf{k}} \varepsilon \cdot \nabla_{\mathbf{r}} f(\mathbf{k}, \mathbf{r}) - \frac{e}{\hbar} \mathbf{E}(\mathbf{r}) \cdot \nabla_{\mathbf{k}} f(\mathbf{k}, \mathbf{r}) = \left[\frac{\partial f(\mathbf{k}, \mathbf{r})}{\partial t} \right]_{ac} + \left[\frac{\partial f(\mathbf{k}, \mathbf{r})}{\partial t} \right]_{iv} \quad (1)$$

where

\mathbf{k} is the electron wave vector; ε is the electron energy; \mathbf{r} is the electron position vector; $f(\mathbf{k}, \mathbf{r})$ is the electron SDMDF in one of the first conduction band valleys; $\mathbf{E}(\mathbf{r})$ is the space-dependent electric field; the subscripts *ac* and *iv* correspond to acoustic and intervalley phonons respectively.

The first term on the left hand side is often considered to give the variation in $f(\mathbf{k}, \mathbf{r})$ which is due to diffusion; the second term gives the effect of electric field; the terms on the right hand side are the collision integrals which describe the effects of the major scattering mechanisms in silicon -- acoustic and intervalley phonon scattering.

To solve Equation (1), while also accounting for the effects of silicon's ellipsoidal energy surfaces, we have to first transform Equation (1) to the starred momentum space (\mathbf{k}^* space), where the constant energy surfaces are spherical[5]. To facilitate our space-dependent solution, we perform the inverse transformation to the position vector \mathbf{r} . The starred electron wave vector \mathbf{k}^* and the starred electric field vector \mathbf{E}^* , as well as the starred position vector \mathbf{r}^* have the following relationship to their original values:

$$\mathbf{k}^* = \bar{\alpha}^{-1/2} \mathbf{k}; \quad \mathbf{E}^* = \bar{\alpha}^{1/2} \mathbf{E}; \quad \mathbf{r}^* = \bar{\alpha}^{-1/2} \mathbf{r} \quad (2)$$

where

$\bar{\alpha}^{-1/2}$ is the well known Herring-Vogt transformation matrix[5].

After transforming the Boltzmann transport equation, we obtain

$$\frac{1}{\hbar} \nabla_{\mathbf{k}^*} \cdot \varepsilon \cdot \nabla_{\mathbf{r}^*} f(\mathbf{k}^*, \mathbf{r}^*) - \frac{e}{\hbar} \mathbf{E}^*(\mathbf{r}^*) \cdot \nabla_{\mathbf{k}^*} f(\mathbf{k}^*, \mathbf{r}^*) = \left[\frac{\partial f(\mathbf{k}^*, \mathbf{r}^*)}{\partial t} \right]_{ac} + \left[\frac{\partial f(\mathbf{k}^*, \mathbf{r}^*)}{\partial t} \right]_{iv} \quad (4)$$

We use the following dispersion relation to account for silicon's non-parabolic band structure:

$$\gamma(\varepsilon) = \varepsilon + \beta \varepsilon^2 = \frac{\hbar^2 \mathbf{k}^{*2}}{2m_0} \quad (5)$$

In this well-known dispersion relation, β is the non-parabolicity factor which has been given the value $\beta = 0.5eV^{-1}$ for silicon [4]. While we have used this popular expression for the band structure, it is important to note that only $\gamma(\varepsilon)$ will be used in our formulation. This alleviates restrictions on allowable dispersion relations to continuous analytical functions of energy.

To transform Equation (4) into a solvable expression, we choose the electric field to be in the symmetrical [111] crystallographic direction[1]. This field direction forces the SD MDF's to be identical in each valley. Furthermore, the position vector is taken to be one-dimensional and parallel to the electric field $\mathbf{E}^*(\mathbf{r}^*)$. Under this condition, the problem will be one-dimensional in real space, and \mathbf{E}^* and \mathbf{r}^* can be replaced by the scalars E^* and x^* . The next step is to express the SD MDF as the sum of the first and second Legendre polynomials multiplied by their respective coefficients[1,6]:

$$f(\mathbf{k}^*, \mathbf{r}^*) = f(\mathbf{k}^*, x^*) = f_0(\varepsilon, x^*) + k^* g(\varepsilon, x^*) \cos \theta \quad (6)$$

where

θ is the angle between $\mathbf{E}^*(x^*)$ and \mathbf{k}^* ; $f_0(\varepsilon, x^*)$ is the coefficient of the first Legendre polynomial which is the symmetrical part of the SD MDF; $k^* g(\varepsilon, x^*)$ is the coefficient of the second Legendre polynomial which is the anti-symmetrical portion of the SD MDF.

To ascertain the SD MDF we must now determine the two unknown functions $f_0(\varepsilon, x^*)$ and $g(\varepsilon, x^*)$. By substituting Equation (6) into Equation (4), we can obtain a tractable form of the Boltzmann equation, which contains both symmetrical and anti-symmetrical parts. By equating symmetrical parts to symmetrical parts, and anti-symmetrical parts to anti-symmetrical parts, and performing algebraic manipulations, two equations are obtained (details in the appendix). These two equations can be solved for the two unknown functions. These equations can be reduced to one equation for the symmetrical part of the SD MDF $f_0(\varepsilon, x^*)$:

$$\begin{aligned}
& \frac{2\sqrt{\gamma(\varepsilon)}\tau_0}{3\gamma'(\varepsilon)^3m_0} \left[\frac{\partial^2 f_0(\varepsilon, x^*)}{\partial x^{*2}} - 2eE^*(x^*) \frac{\partial^2 f_0(\varepsilon, x^*)}{\partial \varepsilon \partial x^*} + (eE^*(x^*))^2 \frac{\partial^2 f_0(\varepsilon, x^*)}{\partial \varepsilon^2} \right] \\
& + \frac{2}{3} \left(1 - \frac{2\gamma(\varepsilon)\gamma''(\varepsilon)}{\gamma'(\varepsilon)^2} \right) \frac{\tau_0 e E^*(x^*)}{\gamma'(\varepsilon)^2 \sqrt{\gamma(\varepsilon)} m_0} \left[e E^*(x^*) \frac{\partial f_0(\varepsilon, x^*)}{\partial \varepsilon} - \frac{\partial f_0(\varepsilon, x^*)}{\partial x^*} \right] \\
& - \frac{2\sqrt{\gamma(\varepsilon)}\tau_0}{3\gamma'(\varepsilon)^3m_0} \frac{e \partial E^*(x^*)}{\partial x^*} \frac{\partial f_0(\varepsilon, x^*)}{\partial \varepsilon} \\
& + \frac{4\sqrt{2}m_t^2 m_l^{1/2} D_{ac}^2}{\pi \hbar^4 \rho} \sqrt{\gamma(\varepsilon)\gamma'(\varepsilon)^2} \left\{ \left[1 + \frac{\gamma(\varepsilon)\gamma''(\varepsilon)}{\gamma'(\varepsilon)^2} \right] f_0(\varepsilon, x^*) \right. \\
& + \left. \left[\frac{\gamma(\varepsilon)}{2\gamma'(\varepsilon)} + \left(1 + \frac{\gamma(\varepsilon)\gamma''(\varepsilon)}{\gamma'(\varepsilon)^2} \right) K_0 T \right] \frac{\partial f_0(\varepsilon, x^*)}{\partial \varepsilon} + \frac{\gamma(\varepsilon) K_0 T}{2\gamma'(\varepsilon)} \frac{\partial^2 f_0(\varepsilon, x^*)}{\partial \varepsilon^2} \right\} \\
& + \sum_{n=1}^{15} \frac{D_n^2 (m_t^2 m_l)^{1/2}}{\sqrt{2\pi} \hbar^3 \rho \omega_n} \left[\frac{1}{e^{\hbar\omega_n/K_0T} - 1} \right] \\
& \times \left\{ \sqrt{\gamma(\varepsilon + \hbar\omega_n)} \gamma'(\varepsilon + \hbar\omega_n) \left[e^{\hbar\omega_n/K_0T} f_0(\varepsilon + \hbar\omega_n, x^*) - f_0(\varepsilon, x^*) \right] \right. \\
& + \left. \sqrt{\gamma(\varepsilon - \hbar\omega_n)} \gamma'(\varepsilon - \hbar\omega_n) \left[f_0(\varepsilon - \hbar\omega_n, x^*) - e^{\hbar\omega_n/K_0T} f_0(\varepsilon, x^*) \right] \right\} \\
& = 0
\end{aligned} \tag{7}$$

where

τ_0 is the proportionality factor which relates the phonon scattering rate to energy. τ_0 has units of $eV^{1/2}sec$ and its values are given in references[1,2]; $\gamma'(\varepsilon)$ and $\gamma''(\varepsilon)$ are the first and the second derivatives of $\gamma(\varepsilon)$ with respect to energy; m_t and m_l are silicon's longitudinal and transverse effective masses respectively; D_{ac} is the acoustic phonon deformation potential; ρ is the density; T is the lattice temperature; K_0 is Boltzmann's constant; D_n is the intervalley phonon deformation potential and the subscript n stands for different kinds of intervalley phonon scattering; ω_n is the intervalley phonon vibrational frequency.

For the second order differential/difference equation given by Expression (7) we formulate a boundary value problem in two dimensions: real space and energy space. The four sets of boundary conditions used to help define the problem are depicted in Figure 1, and are described below:

- (1) The distribution function at $x = 0$, which corresponds to the region where electrons are injected from an ohmic contact, is given by a Maxwellian.
- (2) At $x = l$, which is the right edge of the device, we can use either a Dirchlet condition where the SD MDF is specified, or a Neumann condition with the normal, real-space derivative of the distribution function equal to zero. In the presented calculations, the Dirchlet condition is used, with the requirement that the distribution function is equal to its homogeneous-field limiting value.
- (3) The SD MDF is zero at very large energy, which for our calculations is approximately 1.5eV.
- (4) Since we are assuming there is no generation or recombination, the product of electron concentration and drift velocity $n(x)v(x)$, and therefore current density are constant. The value of current density depends on the doping concentration. We use the requirement of constant current density as a substitute for a boundary condition at $\varepsilon = 0$. The expression for current density $J(x) = en(x)v(x)$ is given in Section 4.

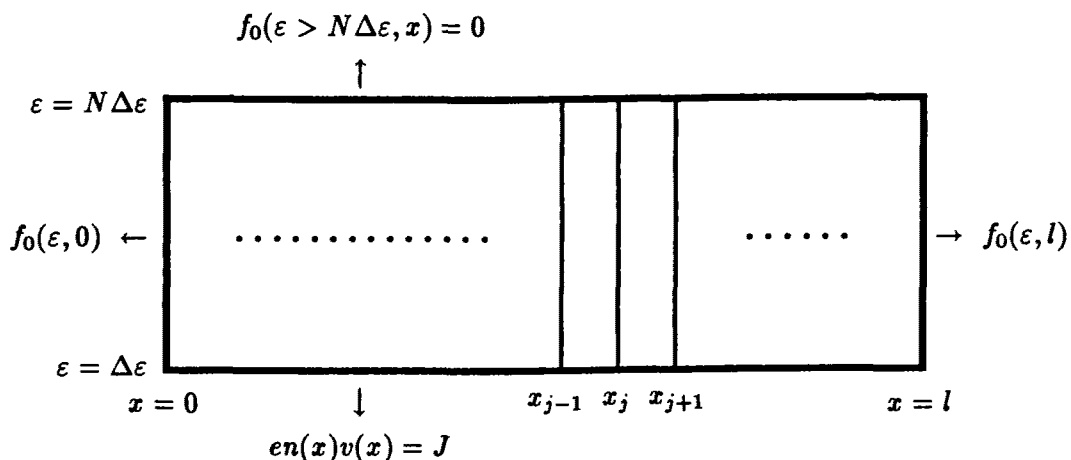


Fig.1. Boundary conditions of the silicon bar are represented: the horizontal direction represents position, while the vertical direction represents energy; at left $f_0(\varepsilon, 0)$ is Maxwellian; at right $f_0(\varepsilon, l)$ is given by the Dirchlet condition; at top $f_0(\varepsilon, x) = 0$; at bottom the current conservation requirement is represented.

3. Numerical Solution

With the analytical expression of the Boltzmann transport equation derived and given by Formula (7), the next step is to apply numerical techniques to obtain the solution, which is the symmetrical part of the distribution function $f_0(\varepsilon, x)$.

The basic strategy we use is to approximate Equation (7) by a system of coupled difference equations, and then solve that system. The first step is to discretize Equation (7) with respect to energy ε and position x^* . We choose a mesh of N points in the energy domain which is equally spaced with increments of $\Delta\varepsilon$. In the real-space domain, we employ a mesh of $M + 1$ points which is narrowly spaced in regions where the SD MDF is rapidly varying, and coarse when its spatial variation is reduced. The resulting grid is a two-dimensional mesh with $N \times (M + 1)$ points. Using the central-difference method, we obtain a difference equation for each point or node. The i, j 'th difference equation is listed below:

$$\begin{aligned}
& \frac{2\sqrt{\gamma_i}\tau_0}{3\gamma_i'^3 m_0} \left[\frac{2(f_{i,j+1} - f_{i,j})}{s_{j+1}(s_j + s_{j+1})} - \frac{2(f_{i,j} - f_{i,j-1})}{s_j(s_j + s_{j+1})} \right] \\
& - \frac{2\sqrt{\gamma_i}\tau_0}{3\gamma_i'^3 m_0} \frac{eE_j^*}{\Delta\varepsilon} \frac{f_{i+1,j+1} - f_{i+1,j-1} - f_{i-1,j+1} + f_{i-1,j-1}}{s_j + s_{j+1}} \\
& + \frac{2\sqrt{\gamma_i}\tau_0}{3\gamma_i'^3 m_0} \left(\frac{eE_j^*}{\Delta\varepsilon} \right)^2 (f_{i+1,j} - 2f_{i,j} + f_{i-1,j}) \\
& - \frac{2}{3} \left(1 - \frac{2\gamma_i\gamma_i''}{\gamma_i'^2} \right) \frac{\tau_0 eE_j^*}{\sqrt{\gamma_i}\gamma_i'^2 m_0} \frac{f_{i,j+1} - f_{i,j-1}}{s_j + s_{j+1}} \\
& - \frac{\tau_0}{\sqrt{\gamma_i}\gamma_i'^2 m_0} \left[\frac{2\gamma_i eE_{j+1}^* - eE_{j-1}^*}{3\gamma_i' s_j + s_{j+1}} - \frac{2}{3} \left(1 - \frac{2\gamma_i\gamma_i''}{\gamma_i'^2} \right) (eE_j^*)^2 \right] \frac{f_{i+1,j} - f_{i-1,j}}{2\Delta\varepsilon} \\
& + \frac{4\sqrt{2}m_i^2 m_l^{1/2} D_{ac}^2}{\pi \hbar^4 \rho} \sqrt{\gamma_i}\gamma_i'^2 \left\{ \left(1 + \frac{\gamma_i\gamma_i''}{\gamma_i'^2} \right) f_{i,j} \right. \\
& + \left[\frac{\gamma_i}{2\gamma_i'} + \left(1 + \frac{\gamma_i\gamma_i''}{\gamma_i'^2} \right) K_0 T \right] \frac{f_{i+1,j} - f_{i-1,j}}{2\Delta\varepsilon} + \frac{\gamma_i}{2\gamma_i'} K_0 T \frac{f_{i+1,j} - 2f_{i,j} + f_{i-1,j}}{\Delta\varepsilon^2} \left. \right\} \\
& + \sum_{n=1}^{15} \frac{D_n^2 (m_i^2 m_l)^{1/2}}{\sqrt{2}\pi \hbar^3 \rho \omega_n} \left\{ \sqrt{\gamma_{i+l_n}}\gamma_{i+l_n}' \left[\frac{e^{\hbar\omega_n/K_0 T} f_{i+l_n,j} - f_{i,j}}{e^{\hbar\omega_n/K_0 T} - 1} \right] \right.
\end{aligned}$$

$$\begin{aligned}
& + \sqrt{\gamma_{i-l_n} \gamma'_{i-l_n}} \left[\frac{f_{i-l_n, j} - e^{\hbar\omega_n/K_0T} f_{i, j}}{e^{\hbar\omega_n/K_0T} - 1} \right] \Big\} \\
& = 0
\end{aligned} \tag{8}$$

where

$f_{i, j}$ is equivalent to $f_0(i\Delta\varepsilon, x_j^*)$ with i and j corresponding to energy and position domains; s_j and s_{j+1} are equal to $x_j^* - x_{j-1}^*$ and $x_{j+1}^* - x_j^*$ respectively. We also assume x_j^* is always less than x_{j+1}^* for any j ; $\Delta\varepsilon$ is a very small energy increment step; l_n is the closest integer to $\frac{\hbar\omega_n}{\Delta\varepsilon}$; $\gamma_i = \gamma(i\Delta\varepsilon)$; $\gamma_{i+l_n} = \gamma(i\Delta\varepsilon + \hbar\omega_n)$; $\gamma'_i = \gamma'(i\Delta\varepsilon)$ is the first derivative of the dispersion relation with respect to energy; $\gamma''_i = \gamma''(i\Delta\varepsilon)$ is the second derivative of the dispersion relation with respect to energy; $E_j^* = E^*(x_j^*)$ is the electric field at x_j^* .

There is an analogous difference equation for each of the $N \times M$ mesh points in the two-dimensional energy/real-space domain. Since the energy domain and the real-space domain are divided into approximately three hundred intervals and sixty intervals respectively, this represents a matrix equation with approximately eighteen thousand rows. A direct solution of this system proved to be computationally inefficient. For this reason, we employ two different techniques simultaneously to obtain a solution. In the real-space domain we use an iterative method (method of lines), and in the energy domain we solve our system of equations directly using a sparse-matrix method which employs a direct technique[7]. The method can be understood by first observing that in Equation (8), the distribution function at the point x_j^* can be determined if the distribution functions at the points x_{j-1}^* and x_{j+1}^* are already known. In other words, if we know $f_0(\varepsilon, x_{j-1}^*)$ and $f_0(\varepsilon, x_{j+1}^*)$, we can solve for $f_0(\varepsilon, x_j^*)$. Of course we do not know $f_0(\varepsilon, x_{j+1}^*)$, so we assume its values and then solve for $f_0(\varepsilon, x_j^*)$. The result will be improved values for $f_0(\varepsilon, x_j^*)$. The procedure is repeated iteratively for all spatial points until the process converges. Numerically, this involves solving an $N \times N$ matrix equation repeatedly. It is interesting to note that this solution technique is facilitated by the physics of the problem. In the energy domain, the various difference equations are strongly coupled over a large energy range by intervalley phonon scattering. With this strong coupling, a direct solution of the matrix equation is prudent. However, in the real-space domain, the difference equations are coupled only to their nearest neighbors, and rapid convergence is obtained using the iterative method described.

One may now obtain a better understanding of the numerical techniques employed by considering the following discussion. For a given point x_j^* in the real-space domain, we have $N - 1$ equations in the energy domain in the form of Equation (8), and one equation which corresponds to the condition of constant current density (condition 4 above). The equations analogous to Equation (8) are enumerated from $i = 2$ to $i = N$, while we place our boundary condition in the first matrix row, which corresponds to the energy point $i = 1$. This set of equations can be expressed by the following matrix equation:

$$\overline{\overline{\mathbf{M}}}_j \overline{\overline{\mathbf{F}}}_j^k = -\overline{\overline{\mathbf{L}}}_{j-1} \overline{\overline{\mathbf{F}}}_{j-1}^k - \overline{\overline{\mathbf{R}}}_{j+1} \overline{\overline{\mathbf{F}}}_{j+1}^{k-1} \tag{9}$$

where

$\overline{\overline{\mathbf{F}}}_j^k$ is a column matrix, which represents the discretized SD MDF at the point x_j^* with the k 'th iteration; $\overline{\overline{\mathbf{F}}}_{j-1}^k$ represents the discretized SD MDF at the point left of x_j^* with the k 'th iteration; $\overline{\overline{\mathbf{F}}}_{j+1}^{k-1}$ represents the discretized SD MDF at the point right of x_j^* with the $k - 1$ 'th iteration.

$\overline{\overline{\mathbf{M}}}_j$, $\overline{\overline{\mathbf{L}}}_{j-1}$ and $\overline{\overline{\mathbf{R}}}_{j+1}$ are the coefficient square matrices of $\overline{\overline{\mathbf{F}}}_j^k$, $\overline{\overline{\mathbf{F}}}_{j-1}^k$ and $\overline{\overline{\mathbf{F}}}_{j+1}^{k-1}$ respectively.

All the values on the right hand side of Equation (9) are presumed to be known, so \overline{F}_j^k can be obtained using the sparse matrix solution algorithm[7]. Once \overline{F}_j^k is obtained, we use it to obtain an improved value for the distribution function at the next point in the space domain \overline{F}_{j+1}^k . We perform this calculation for each real-space point until we reach the end of the real-space domain. The process is then repeated until it converges. To make this process converge faster, we have also used the SOR method with a relaxation factor of approximately 1.4[8].

4. Averages of the Distribution Function

Traditional device simulation provides values of average transport quantities which often include carrier concentration $n(x)$, current density $J(x)$, and average energy $\varepsilon(x)$. While the solution to the BTE provides the entire distribution function, it is often useful to calculate average quantities. After finding the SDMDF, we can use it to find any relevant average value by simple integration. Here we present values for $n(x)$, which is calculated by integrating the SDMDF over all momentum space, and $J(x)$ and $\varepsilon(x)$ which are determined by the following integrations:

$$\varepsilon(x^*) = \frac{1}{4\pi^3 n(x^*)} \int \varepsilon(k) f(\mathbf{k}, x^*) d\mathbf{k}; \quad n(x^*) \mathbf{v}(x^*) = \frac{\mathbf{J}}{e} = \frac{1}{4\pi^3} \int \mathbf{v}(\mathbf{k}) f(\mathbf{k}, x^*) d\mathbf{k} \quad (10)$$

A discussion of calculated values and their comparison with analogous Monte Carlo based simulations is given below.

5. Results

To analyze the accuracy of our new method for determining the SDMDF, we performed a series of calculations. In these calculations our semiconductor device is a silicon bar of length $0.2\mu m$, at the lattice temperature of $300^\circ K$ with a constant applied potential. We assume that the electric field within the bar is spatially constant. Electrons are injected into the bar with an equilibrium Maxwellian distribution at $x = 0$, as they would be from an ohmic contact. Electrons then gain energy from the field, and the SDMDF varies along the device until it reaches its homogeneous-field limiting value. We normalize the SDMDF to have a carrier concentration of $10^{17} cm^{-3}$ in the homogeneous-field limit.

Figure 2 shows the distribution function at different positions for an electron ensemble which is in the presence of a constant electric field with a magnitude of $100kV/cm$. It is interesting to note that the distribution spreads over a wider energy range as the electron ensemble drifts toward the far electrode. Eventually, the distribution function reaches its non-Maxwellian homogeneous field limit.

Figure 3 shows the product of the distribution and the density of states at different points throughout the device, for a field magnitude of $100kV/cm$. From the figure it is clear that electrons obtain more and more energy as x increases, so the peak of this 3-D plot is moving from low energy at small distances to higher energy at larger distances.

In Figure 4 we give the results of investigations involving average velocity and carrier concentration. Values for the electron drift velocity (solid curve) and the carrier concentration (dashed curve) are plotted as a function of position for an electric field of $100kV/cm$. As expected, the product of velocity and concentration is constant, which satisfies the continuity equation ($\frac{\partial}{\partial x} (n(x)v(x)) = 0$). In addition, we compare our values for drift velocity with those calculated by Monte Carlo simulations[9] (open circles). Agreement between the two methods is usually within 5%, and both techniques predict velocity overshoot which is characteristic of nonequilibrium electron transport.

In Figure 5 we show values for average energy which were calculated using the SDMDF. As is expected, average electron energy values (solid curves) increase gradually with distance until they reach the homogeneous-field limit. The figure shows the results of calculations for three different electric field magnitudes: $20kV/cm$, $60kV/cm$ and $100kV/cm$. We performed similar calculations

using the Monte Carlo program which are plotted as open circles. The figure indicates that the two methods are in excellent agreement.

5. Conclusion

We have solved the space-dependent Boltzmann transport equation to obtain the space-dependent momentum distribution function. The method, which expands upon an earlier space-independent technique[1], uses Legendre polynomials to formulate a space-dependent Boltzmann equation. The resulting partial differential/difference form of the Boltzmann equation is then solved numerically. The numerical technique uses a novel combination of a direct sparse matrix algorithm and an iterative technique. In addition to space dependence, the effects of inelastic phonon scattering and non-parabolic band structure are included in our formulation. With this approach, the SD-MDF's are calculated faster than those obtained from Monte Carlo calculations. With accurate SD-MDF's determined, space-dependent values for average electron energy, electron drift velocity, and carrier concentrations were obtained which agree well with those obtained from Monte Carlo simulations. In addition to calculating these average quantities, the technique gives the entire distribution function which is important for modeling MOSFET reliability, EPROM programming, and HEMT performance. In summary, we have presented an accurate method for solving the Boltzmann transport equation which is sufficiently economical for daily use in device simulation.

Acknowledgements – The authors are grateful to Shih-Luen Wang and Ken Hennacy for helpful discussions. This work was supported in part by the Semiconductor Research Corporation under contract no. 91-DJ-130, and the National Science Foundation under contract no. ECS-9010457.

References

- [1] N. Goldsman, L. Henrickson and J. Frey, *Solid-State Electronics*, Vol. 34, p. 389 (1991).
- [2] N. Goldsman, Y. J. Wu and J. Frey, *J. Appl. Phys.*, **68**, p.1075(1990).
- [3] H. Lin and N. Goldsman, to be published on *Solid-State Electronics*.
- [4] C. Jacoboni and L. Reggiani, *Reviews of Modern Physics*, **55**, p.645(1983).
- [5] Conyers Herring and Erich Vogt, *Physical Review*, **101**, p.944(1956).
- [6] E. M. Conwell and M. O. Vassel, *Physical review*, **166**, p.797(1968).
- [7] Alan George, Joseph Liu, and Esmond Ng, *SPARSPAK User Guide: Waterloo Sparse Linear Equation Package*, Department of Computer Science, University of Waterloo, Waterloo, Ontario, Canada(1980).
- [8] W. F. Ames, "Numerical Methods for Partial Differential Equations," 2nd. ed., Academic Press, New York(1977).
- [9] N. Goldsman and J. Frey, *IEEE Trans. Elec. Dev.*, Vol. 35, p. 1524 (1988).

Appendix Derivation of Boltzmann Transport Equation

To derive the space-dependent Boltzmann equation (Equation (7)), we start from Equation (4) which is the Boltzmann equation transformed into the starred phase-space, which has six dimensions: three in momentum space, and three in real space. A six-dimensional analysis is indeed cumbersome, so we limit our real-space analysis to one dimension, and we change our real-space variable from \mathbf{r}^* to the one-dimensional position variable x^* . The direction of x^* , with the unit vector denoted as \hat{x}^* , is parallel to the transformed electric field $\mathbf{E}^*(x^*)$.

As was mentioned in Section 2, we divide our solution into symmetrical and anti-symmetrical components. In order to obtain a closed set of equations in this analysis, we decompose \mathbf{k}^* into \mathbf{k}_\perp^* and k_\parallel^* which are the wave vectors perpendicular and parallel to $\mathbf{E}^*(x^*)$ respectively. By using the dispersion relation given by Equation (5) we then make the following approximation which has been justified in the space-independent case by comparison with Monte Carlo calculation[1].

$$\frac{\gamma(\varepsilon)}{3} = \frac{\hbar^2 k_\parallel^{*2}}{2m_0} \quad (11)$$

From the dispersion relation, the derivative of energy with respect to \mathbf{k}^* can be expressed as another form which is

$$\nabla_{\mathbf{k}^*} \varepsilon = \frac{\hbar^2 \mathbf{k}^*}{\gamma'(\varepsilon) m_0} \quad (12)$$

With the above equation, as well as the chain rule, Equation (4) can be written as an expression in four-dimensional phase-space:

$$\frac{\hbar \mathbf{k}^*}{\gamma'(\varepsilon) m_0} \cdot \hat{x}^* \frac{\partial}{\partial x^*} f(\mathbf{k}^*, x^*) - e E^*(x^*) \hat{x}^* \cdot \frac{\hbar \mathbf{k}^*}{\gamma'(\varepsilon) m_0} \frac{\partial}{\partial \varepsilon} f(\mathbf{k}^*, x^*) = \left[\frac{\partial f(\mathbf{k}^*, x^*)}{\partial t} \right]_{coll} \quad (13)$$

where

the term on the right hand side represents the expressions for acoustic and intervalley phonon scattering.

To facilitate our formulation, we limit our specification of momentum space to directions perpendicular and parallel to the electric field. We then use Legendre polynomials to express the distribution function as the sum of its symmetrical and anti-symmetrical components, and then substitute this expression, which is Equation (6) with $k_\parallel^* = k^* \cos\theta$, into Equation (13). After some mathematical manipulations, the following expression is obtained:

$$\begin{aligned} & \frac{\hbar k_\parallel^*}{\gamma'(\varepsilon) m_0} \left[\frac{\partial f_0(\varepsilon, x^*)}{\partial x^*} + k_\parallel^* \frac{\partial g(\varepsilon, x^*)}{\partial x^*} \right] - \frac{e E^*(x^*)}{\hbar} \left[\frac{\hbar^2 k_\parallel^*}{\gamma'(\varepsilon) m_0} \frac{\partial f_0(\varepsilon, x^*)}{\partial \varepsilon} \right. \\ & \left. + g(\varepsilon, x^*) + \frac{\hbar^2 k_\parallel^{*2}}{\gamma'(\varepsilon) m_0} \frac{\partial g(\varepsilon, x^*)}{\partial \varepsilon} \right] = \left[\frac{\partial f_0(\varepsilon, x^*)}{\partial t} \right]_{coll} - \frac{k_\parallel^* g(\varepsilon, x^*)}{\tau(\varepsilon)} \end{aligned} \quad (14)$$

where

the collision term on the right hand side of Equation (14) has been separated into its symmetrical and anti-symmetrical components; k_\parallel^* and $E^*(x^*)$ are the magnitude of \mathbf{k}_\parallel^* and $\mathbf{E}^*(x^*)$ respectively.

$\frac{1}{\tau(\varepsilon)}$ is the summation of all acoustic and intervalley scattering rates. In reference[1], $\tau(\varepsilon)$ is shown to be well approximated by

$$\tau(\varepsilon) = \frac{\tau_0}{\gamma'(\varepsilon)\sqrt{\gamma(\varepsilon)}} \quad (15)$$

where τ_0 represents all the coupling factors for deformation potential scattering. The approximate values of $\frac{1}{\tau_0}$ are the slopes of the curve obtained by plotting total scattering rate versus $\gamma'(\varepsilon)\sqrt{\gamma(\varepsilon)}$ [1,2]:

By equating the terms of the same Legendre polynomial order, and using Equation (15), we eliminate the independent variable k_{\parallel}^* , and obtain the following two equations from which to determine the unknown functions $f_0(\varepsilon, x^*)$ and $g(\varepsilon, x^*)$:

$$\frac{\hbar}{\gamma'(\varepsilon)m_0} \left[\frac{\partial f_0(\varepsilon, x^*)}{\partial x^*} - eE^*(x^*) \frac{\partial f_0(\varepsilon, x^*)}{\partial \varepsilon} \right] = -\frac{\gamma'(\varepsilon)\sqrt{\gamma(\varepsilon)}}{\tau_0} g(\varepsilon, x^*) \quad (16.1)$$

$$\frac{1}{\hbar} \left\{ \frac{2\gamma(\varepsilon)}{3\gamma'(\varepsilon)} \frac{\partial g(\varepsilon, x^*)}{\partial x^*} - eE^*(x^*) \left[g(\varepsilon, x^*) + \frac{2\gamma(\varepsilon)}{3\gamma'(\varepsilon)} \frac{\partial g(\varepsilon, x^*)}{\partial \varepsilon} \right] \right\} = \left[\frac{\partial f_0(\varepsilon, x^*)}{\partial t} \right]_{coll} \quad (16.2)$$

To eliminate $g(\varepsilon, x^*)$ from the above two equations, we substitute Equation(16.1) into Equation (16.2) and obtain an equation which only contains the symmetrical part of the distribution function:

$$\begin{aligned} & -\frac{2\sqrt{\gamma(\varepsilon)}\tau_0}{3\gamma'(\varepsilon)^3m_0} \left[\frac{\partial^2 f_0(\varepsilon, x^*)}{\partial x^{*2}} - 2eE^*(x^*) \frac{\partial^2 f_0(\varepsilon, x^*)}{\partial \varepsilon \partial x^*} + (eE^*(x^*))^2 \frac{\partial^2 f_0(\varepsilon, x^*)}{\partial \varepsilon^2} \right] \\ & + \frac{2}{3} \left(1 - \frac{2\gamma(\varepsilon)\gamma''(\varepsilon)}{\gamma'(\varepsilon)^2} \right) \frac{\tau_0 e E^*(x^*)}{\gamma'(\varepsilon)^2 \sqrt{\gamma(\varepsilon)} m_0} \left[\frac{\partial f_0(\varepsilon, x^*)}{\partial x^*} - eE^*(x^*) \frac{\partial f_0(\varepsilon, x^*)}{\partial \varepsilon} \right] \\ & + \frac{2\sqrt{\gamma(\varepsilon)}\tau_0}{3\gamma'(\varepsilon)^3m_0} \frac{e \partial E^*(x^*)}{\partial x^*} \frac{\partial f_0(\varepsilon, x^*)}{\partial \varepsilon} = \left[\frac{\partial f_0(\varepsilon, x^*)}{\partial t} \right]_{coll} \end{aligned} \quad (17)$$

The formulated Boltzmann Equation (7) can now be obtained by providing explicit expressions for the acoustic and intervalley collision terms. These terms have already been derived, and can be found in reference[1]. Equation (7) is thus obtained substituting the appropriate expressions for the collision term into Equation (17).

After Equation (7) is solved numerically, the distribution function, which is in the starred space, is transformed to the original space to obtain a physically relevant solution.

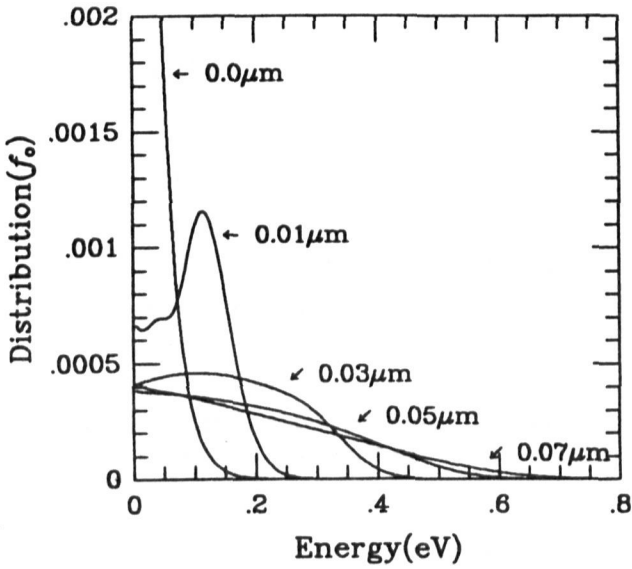


Fig. 2. Electron energy distribution function for electric field value of 100 kV/cm at various positions marked by arrows.

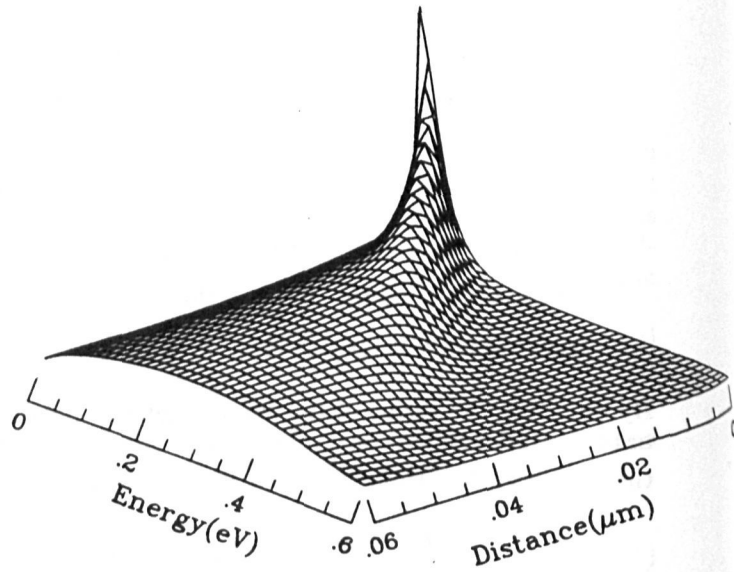


Fig. 3. Electron distribution function versus energy and distance forms this 3-D picture for the electric field value of 100 kV/cm . The distribution function has been multiplied by the density of states.

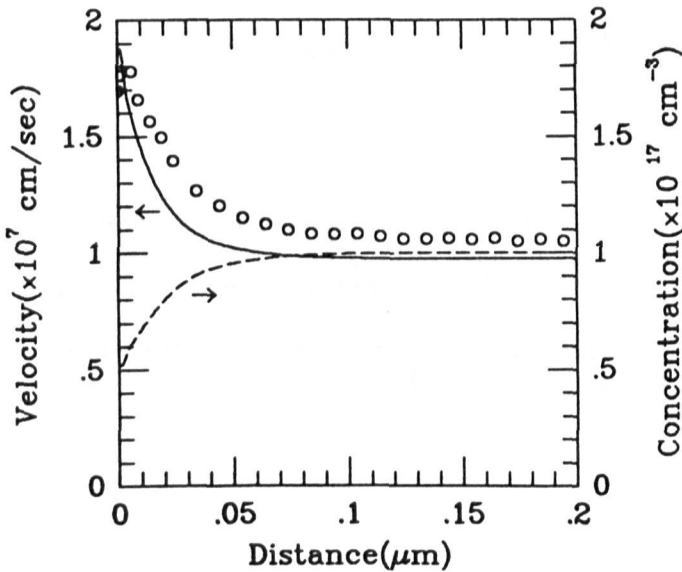


Fig. 4. The space-dependent average electron drift velocity calculated by the SDMDF (solid line) is compared with electron drift velocity calculated by Monte Carlo method (open circles) for the electric field value of 100 kV/cm . The dashed line is the space-dependent concentration obtained from the SDMDF.

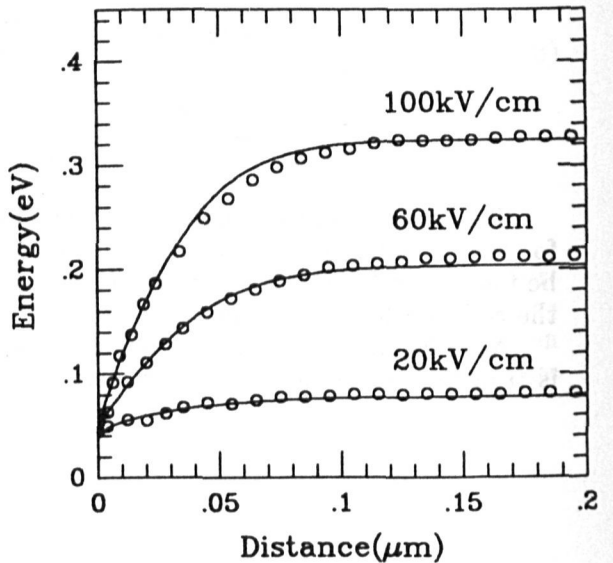


Fig. 5. The average electron energy calculated by the SDMDF (solid lines) is compared with average energy calculated by Monte Carlo simulation (open circles) for different electric field values of 20 kV/cm , 60 kV/cm and 100 kV/cm .